RSC Advances

PAPER

View Article Online
View Journal | View Issue

Cite this: *RSC Adv.*, 2021, **11**, 739

A dual enhanced anti-bacterial strategy based on high chlorin e6-loaded polyethyleneimine functionalized graphene†

Jiangxia Wang,[a] Yuting Yang,[a] Yuanliang Xu,[b] Lifeng Zhao,[a] Lu Wang,[a] Zhengzhi Yin,[c] Huiming Li,*[b] Huan Tan*[a] and Kunping Liu *[a]

Received 18th September 2020
Accepted 30th November 2020

DOI: 10.1039/d0ra07976f

rsc.li/rsc-advances

Bacterial infection has always been a long-term problem of human history and has nowadays became a severe threat to human health with the appearance of drug-resistant bacteria due to the abuse of antibiotics. In this study, a high chlorin e6 (Ce6) photosensitizer-loaded polyethyleneimine-functionalized graphene (PEI-G) nanocomposite (PEI-G@Ce6) was prepared. The loading capacity of Ce6 on PEI-G@Ce6 was approximately up to 32.91 wt%, which was higher than that of other nanomaterials. The as-prepared PEI-G@Ce6 not only improves the photostability of free photosensitizer Ce6 molecules but also maintains the ability of singlet oxygen generation. Based on the dual enhancement of the physical antibacterial effects of PEI-G and the photodynamic therapy (PDT) antibacterial effects of loaded photosensitizer Ce6, PEI-G@Ce6 exhibited enhanced antibacterial efficiency towards *Staphylococcus aureus*. Therefore, the present strategy provided an effective platform to improve antibacterial efficiency for the better treatment of wound infections.

1. Introduction

Bacterial infection, which has resulted in the widespread of pathogens and infectious diseases, was always a long-term problem that has accompanied human developing history. The appearance of antibiotics, such as carbapenem, fluoroquinolones, trimethoprim, chloramphenicol and β-lactam, supplied an effective tool to counteract the threat of bacterial infections. However, over the past decades, due to the abuse of antibiotics, numerous pathogens have exhibited resistance towards many antibiotics particularly when further accelerated by the simultaneous use of different antibiotics. One coping strategy is to develop new chemical structure antibiotics with a new antibacterial mechanism. Fortunately, some alternative antibiotics such as aminoglycosides derivatives, peptidomimetics and FimH inhibitors have been developed and obtained fine antibacterial effects.[1–3] However, these antibiotics still suffer from drug-resistance owing to the rapid bacterial evolution. Another strategy is to develop a novel antibacterial pattern different from antibiotics, and numerous attempts have been done, achieving significant development.[4–6] Among them, antimicrobial nanomaterial-based methods, such as widely studied metal and metal oxide nanoparticles (*e.g.*, Ag, Au and ZnO), have attracted considerable attention due to the fine antimicrobial activity and unique properties.[7,8] However, the release of metal ions from metal or metal oxide nanoparticles have brought health risk; hence, a safer substitutable antimicrobial nanomaterial is needed. In addition, photodynamic therapy (PDT)-based methods also got significant interest due to its special antimicrobial mechanism.[9,10] PDT is a photochemistry-based technology activated by light irradiation to generate singlet oxygen ($^1O_2$) under the presence of a photosensitizer and oxygen.[11,12] $^1O_2$ shows a broad-spectrum antimicrobial activity and cannot easily generate drug resistance, which makes PDT a potential tool for resisting bacterial infections.[13,14] Moreover, due to the high $^1O_2$ generated ability and fine photo properties, chlorin e6 (Ce6) is the most commonly used photosensitizer in PDT. However, the nonspecific accumulation of the photosensitizer causes damage to the normal tissues, thus blocking the further clinical application.[15,16] To overcome the above-mentioned challenges, we need to develop a new antimicrobial strategy suitable for clinical applications. Graphene or functionalized graphene nanomaterials has been proven to own superior broad-spectrum antibacterial properties for Gram-positive and Gram-negative bacteria even for fungal pathogens,[17,18] and it can also avoid the development of bacterial drug-resistance caused by the excess use of antibiotics.[19] Thus, graphene or functionalized graphene is an ideal substitutable antimicrobial nanomaterial. Considering the high specific

[a]*Key Laboratory of Medicinal and Edible Plants Resources Development of Sichuan Education Department, Sichuan Industrial Institute of Antibiotics, Chengdu University, Chengdu, 610106, China. E-mail: liukunping@cdu.edu.cn*

[b]*College of Food and Biological Engineering, Chengdu University, Chengdu, 610106, China*

[c]*College of Biological, Chemical Sciences and Engineering, Jiaxing University, Jiaxing, 314001, China*

† Electronic supplementary information (ESI) available. See DOI: 10.1039/d0ra07976f

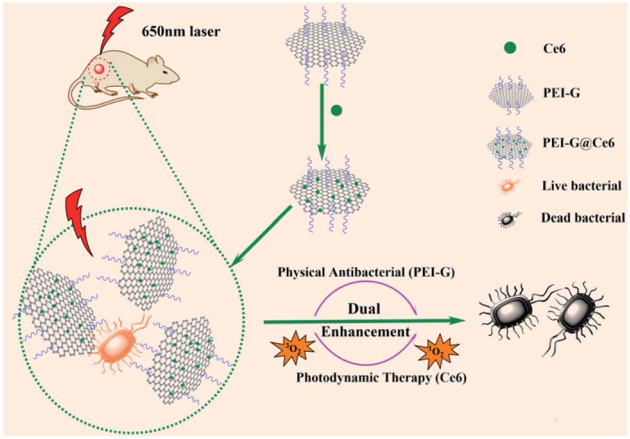

Scheme 1 Schematic of Ce6-loaded polyethyleneimine-functionalized graphene hybrid fabrication and dual enhancement antimicrobial mechanism.

surface area and the π–π conjugated structure of graphene for increasing the loading amount and stability of photosensitizer Ce6, a high Ce6 photosensitizer-loaded polyethyleneimine-functionalized graphene (PEI-G) nanocomposite (PEI-G@Ce6) was prepared for effective PDT against *Staphylococcus aureus* (*S. aureus*) (Scheme 1). Based on the high amount of Ce6 loaded on PEI-G and the dual enhancement of the physical antibacterial effects of PEI-G and PDT antibacterial effects of the loaded photosensitizer Ce6, it was expected that the antibacterial efficiency could be enhanced and the side effects of the photosensitizer could be restricted.

2. Experimental

2.1 Chemicals and characterization

All reagents were of analytical grade and used without further purification. Solutions were prepared using ultra-pure water with a resistance of 18 MΩ cm by a Milli-Q system. 1,3-Diphenylisobenzofuran (DPBF) was purchased from Shanghai Titan Scientific CO., Ltd. Ce6 was bought from Frontier Scientific. The strain of *S. aureus* was CMCC 26003 purchased from the National Institutes for Food and Drug Control. PEI (branched, $M_w = 25\,000$), 96-well cell culture plates, cell culture dishes and centrifuge tubes were obtained from Corning. The FT-IR and UV-Vis spectra were recorded using an Is10 FT-IR apparatus of Thermo Fisher in the spectral range of 400–4000 cm^{-1} and an UV-2600 UV-vis spectrophotometer in the wavelength range from 200 to 700 nm. The morphologies of the samples were characterized by a JSM-7500F field emission scanning electron microscope (SEM) and Tecnai G2 F20 S-TWIN field emission transmission electron microscope (TEM). Raman spectra were recorded on a LabRAM HR (Horiba, France) laser Raman spectrometer and X-ray powder diffraction was performed on XD-3A (Shimadzu).

2.2 Preparation of PEI-G

The preparation of PEI-G is referred to the method in our previous study.[20] Briefly, PEI-G was prepared by a one-step process, and PEI acted as both a reducing agent and a functionalizing agent. First, 30 mL of exfoliated graphene oxide (EGO) dispersion (0.5 mg mL^{-1}) was added to 30 mL of pure water and sonicated until completely dispersed. Continuously, 30 mL of PEI (1% aqueous solution) was added and stirred to a homogeneous solution. Then, the solution was heated to 95 °C for 24 h. After that, the mixture was cooled to room temperature and washed 3 times with pure water to remove redundant PEI. The as-prepared PEI-G was then dispersed in 15 mL of pure water and stored at 4 °C for further use.

2.3 Preparation of PEI-G@Ce6

First, 10 mL of the as-prepared PEI-G (1 mg mL^{-1}) was washed 3 times with DMF to remove residual water and then dispersed in 16 mL of DMF. Subsequently, 4 mL of photosensitizer Ce6 (5 mg mL^{-1} in DMF) was added and reacted at room temperature under stirring for 24 h in dark. After washing three times with DMF to remove redundant Ce6 and three times with water to remove redundant DMF, the as-prepared PEI-G@Ce6 was dispersed in 20 mL ultra-pure water and stored at 4 °C for further use. In addition, all supernatants in DMF washing steps were merged together for the quantification of unreacted free Ce6 using UV-vis absorption band at 404 nm to calculate the loading amount of Ce6 onto the surface of PEI-G.

2.4 Detection of the photostability

The change in UV-vis absorption peaks of the PEI-G@Ce6 nanocomposites and free Ce6 after illumination was examined to evaluate the difference in photostability. Briefly, PEI-G@Ce6 and free Ce6 solution (both contain same final concentration of Ce6 about 10 μg mL^{-1}) were transferred to a quartz cuvette and irradiated several times by a 650 nm lamp for different time intervals. After each irradiation, the UV-vis absorption peak of Ce6 at 404 nm was measured.

2.5 Detection of singlet oxygen generation

DPBF is used as a chemical probe for detecting singlet oxygen generation. The principle is that DPBF will capture the singlet oxygen produced by the photosensitizer molecules after illumination, so the DPBF absorption peak at 410 nm will decrease. Briefly, 2.8 mL DPBF (0.03 mg mL^{-1} in DMSO) was added to the free Ce6 or nanocomposite PEI-G@Ce6 (both contain same final amount of Ce6 about 0.33 μg mL^{-1}) and transferred to a quartz cuvette. Then, the quartz cuvette was irradiated several times by a 650 nm lamp for different time intervals. After each irradiation, the UV-vis absorption peak of DPBF at 410 nm was measured.

2.6 Bacterial viability test

S. aureus was used to evaluate the antibacterial activity of the composite nanomaterial PEI-G@Ce6 and PEI-G. *S. aureus* was cultured in a lysogeny broth (LB) at 37 °C for 24 h under constant shaking at 200 rpm. Then, the bacterium was diluted with LB and transferred to a 96-well plate with a final bacteria concentration of 10^6 CFU mL^{-1} in each well (the optical density

(OD) value at 630 nm of the bacteria was about 0.05). After the addition of different concentrations of PEI-G@Ce6 and PEI-G, the bacteria was cultured for another 2 h at 37 °C, and the OD value at 630 nm of the bacteria was measured as the 2 h data. Next, a 650 nm wavelength LED lamp with a light intensity of 15 000 LUX was used as the light source to irradiate the bacterium in the 96-well plate for 30 min and then keep a continuous culture in 37 °C. Finally, the OD value at 630 nm of the bacteria was measured in a microplate reader every 2 h to map the growth curve of the bacteria. Moreover, for the intuitive evaluation of the effect of PEI-G@Ce6 to the number of viable bacteria after irradiation, the bacteria in the above 96-well plate were transferred to a solid agar medium with a certain dilution factor after 10 h. Then, the coating plate were cultured for another 24 h at 37 °C and the growth situation of live bacteria was recorded by a digital camera.

2.7 Animal wound infection model and histological analysis

All of the procedures were carried out in accordance with the guidelines issued by Chengdu University and Sichuan Province. All of the experiments were approved by the Animal Ethics Committee of Chengdu University. All mice were randomly divided into four groups with three mice in each group and the dorsal of each mouse was scalded to form a new wound of about 6 mm^2 in area. After 24 h, the wounds of the mice were infected by *S. aureus* and the mice were left as they were for another 24 h. Then, the wounds of three groups of mice were treated with PEI-G@Ce6, PEI-G and Ce6, and each group was labelled as it was treated. Simultaneously, nothing was done for the last one group and it was labelled as the control group. Subsequently, the wounds of the mice in PEI-G@Ce6 and Ce6 groups were irradiated by 650 nm light for 30 min. Next, every two days, the images of the wounds of all mice were captured to evaluate the healing status of the wound of mice, and the body weights of each mice were also recorded to evaluate the life status. On day 18, all the mice were sacrificed and dissected to collect the heart, liver, spleen, lungs, kidneys and wound. All collected tissues were fixed in a formalin solution and then embedded, sectioned and stained for the hematoxylin and eosin (H&E) staining observation.

3. Results and discussion

3.1 Characterization of PEI-G and PEI-G@Ce6

PEI-G was prepared by a facile one-pot synthesis method referred to in our previous study.[20] In the study, PEI was used as a bifunctional reagent for reducing and wrapping the EGO sheets to maintain the single layer status of graphene without aggregation. The UV-vis, XRD and Raman spectroscopy techniques were used to prove the successful preparation of PEI-G (Fig. S1A–C†). According to the FT-IR spectrum (Fig. S1D†), after the reduction of EGO, no oxo-group was observed in pure graphene and PEI-G. After the functionalization of Ce6 to PEI-G, the carboxyl group located at 1730 cm^{-1} was observed, which hinted at the successful preparation of PEI-G@Ce6. The SEM and TEM images of PEI-G (Fig. S2†) show that PEI-G has an irregular sheet-like structure, and all sheets are of single layer and keep separation with each other. From the size distribution in the inset of Fig. S2B,† the diameter of PEI-G ranged from 50 nm to 500 nm, which is very suitable for clinical applications. Next, considering the positive electric property and the large π system of PEI-G, the electronegative photosensitizer Ce6 was attached onto the surface of PEI-G to obtain the PEI-G@Ce6 nanocomposite *via* the electrostatic attractions and π–π conjugation effects. After the loading of Ce6 onto the PEI-G surface as the UV-vis shown in Fig. 1A, except the characteristic absorption band of PEI-G, the PEI-G@Ce6 also displayed intensive characteristic peaks of Ce6 at 413 nm, 510 nm and 669 nm. Moreover, due to the π-π conjugation between PEI-G and Ce6, all these peaks had a red shift compared with Ce6, which indicated the successful assembly of Ce6 on the surface of PEI-G. In addition, from the change in the zeta potential shown in Fig. 1B, after the electropositive functionalization of PEI, the zeta potential of PEI-G reversed to +40.7 mV compared with EGO of −36 mV. Then, when Ce6 was loaded onto the surface of PEI-G, the Zeta potential of PEI-G@Ce6 had a small decrease to +32.6 mV because of the electrostatic neutralization of electronegative Ce6, which was also the other obvious evidence for the successful preparation of PEI-G and PEI-G@Ce6 composite. For clinical applications, the solubility of PEI-G@Ce6 indeed is an important factor. From the image of PEI-G@Ce6 (a), PEI-G (b), Ce6 (c) and EGO (d) solution in the inset of Fig. 1B, PEI-G@Ce6, PEI-G and EGO all were homogenous dispersions, which indicated the fine solubility in water of these three nanomaterials. However, Ce6 was insoluble in water and precipitated at the bottom of the vial. Therefore, this insolubility of Ce6 blocks its clinical applications. However, when Ce6 was functionalized on PEI-G, the fine solubility of PEI-G@Ce6 made it possible for clinical applications. According to the quantification of unreacted free Ce6 using UV-vis at 404 nm to the merged washing supernatants generated in the preparation process of PEI-G@Ce6, the loading capacity of Ce6 on PEI-G@Ce6 was approximately up to 32.91 wt%, which was higher than other nanomaterials reported in published articles (Table S1†). This result maybe benefited from the large surface area of PEI-G.

3.2 Antibacterial activity of PEI-G

Next, *S. aureus* was selected as the model bacteria to evaluate the antibacterial activity of PEI-G. PEI-G with different

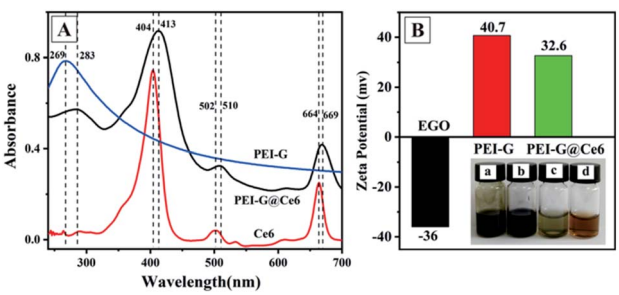

Fig. 1 UV-vis (A) spectrum of Ce6, PEI-G and PEI-G@Ce6 and zeta potential (B) of EGO, PEI-G and PEI-G@Ce6. Inset of B was the image of PEI-G@Ce6 (a), PEI-G (b), Ce6 (c) and EGO (d) solution.

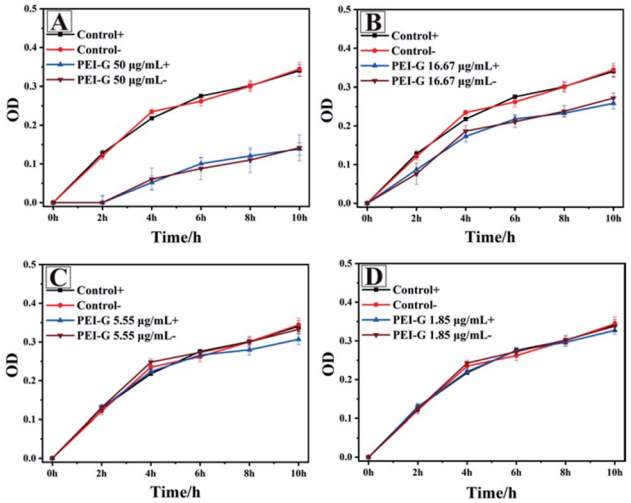

Fig. 2 *S. aureus* inhibition by PEI-G with concentrations of 50.00 (A), 16.67 (B), 5.55 (C) and 1.85 (D) μg mL^{-1} (+ is the illumination group, − is the non-illumination group and the control group has no PEI-G added).

concentrations (50.00, 16.67, 5.55 and 1.85 μg mL^{-1}) were first cultured with *S. aureus* at 37 °C for different times and then the OD value at 630 nm was measured by a microplate spectrophotometer to get the bacterial growth curve (Fig. 2). Moreover, all experiments were divided into a non-illumination group (−) and an illumination group (+) to compare the effects of illumination to antibacterial activity in which the illumination group was irradiated by the 650 nm wavelength LED lamp (with light intensity of 15 000 LUX) for 30 min after the first bacteria co-culture of PEI-G. In the absence of PEI-G (control group), which can be used for the evaluation of the potential risk of killing the bacteria by light irradiation alone, it showed that the light irradiation used in the experiment did not affect the growth of *S. aureus* (control +). For PEI-G, it can be seen that within the concentration range between 50.00 and 16.67 μg mL^{-1}, PEI-G exhibited better antibacterial activity towards *S. aureus* than it exhibited at a lower concentration, which reflected the concentration dependence of *S. aureus* inhibition towards PEI-G. This inhibition of PEI-G towards *S. aureus* should be attributed to the high electrical conductivity of PEI-G because electrical conductivity is known to be one of the factors determining the antibacterial activity against bacteria.[12,21] Meanwhile, due to the fact that PEI-G had a strong positive charge on its surface and the bacteria surface carried a small amount of negative charge from phosphoric acid, PEI-G can bind to the surface of bacteria, leading to the damage of the bacterial cell wall and membrane, eventually causing bacterial death. Moreover, it also could be seen that the illumination had no effect on the antibacterial ability of PEI-G, which hinted that only one physical antibacterial effect exists for PEI-G.

3.3 Photostability and $^1O_2$ generation capacity of Ce6 and PEI-G@Ce6

Electronegative photosensitizer Ce6 attached to the PEI-G@Ce6 nanocomposite was prepared, and the photostability and $^1O_2$ generation capacity of Ce6 and PEI-G@Ce6 were investigated. As the photostability shown in Fig. 3A (UV-vis spectrum was shown in Fig. S3A and S3B†), after 30 min, the UV-vis absorbance intensity of Ce6 dropped down to 45% that of the initial value. However, for PEI-G@Ce6, it still keeps 95% of the absorbance intensity compared with that of the initial value. This phenomenon indicated the great improvement of Ce6 after it was assembled on the surface of PEI-G. Moreover, the ability of PEI-G@Ce6 and Ce6 to produce $^1O_2$ was also investigated using DPBF as the singlet oxygen capture probe. As shown in Fig. 3B (UV-vis spectrum was shown in Fig. S3C and D†), under the light irradiation of 650 nm, although the $^1O_2$ production speed by PEI-G@Ce6 was slightly weaker than that of free Ce6 during the first 3 min which may be owing to the slight holding of PEI-G to $^1O_2$ production, and both PEI-G@Ce6 and Ce6 could quickly produce $^1O_2$ that reflected that both of them had the effective ability for $^1O_2$ production.

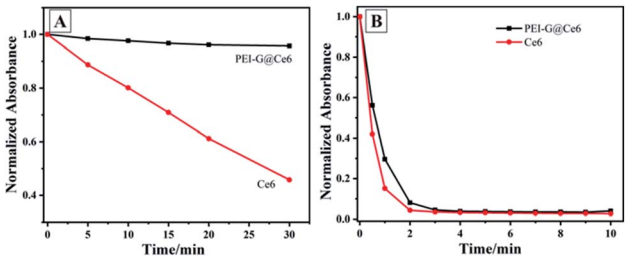

Fig. 3 (A) Photostability and (B) singlet oxygen generation capacity of Ce6, PEI-G@Ce6.

3.4 Antibacterial activity of PEI-G@Ce6

After detection of optical properties, the antibacterial activity of PEI-G@Ce6 towards *S. aureus* was also investigated using the same method as the PEI-G. The bacterial growth curve is shown

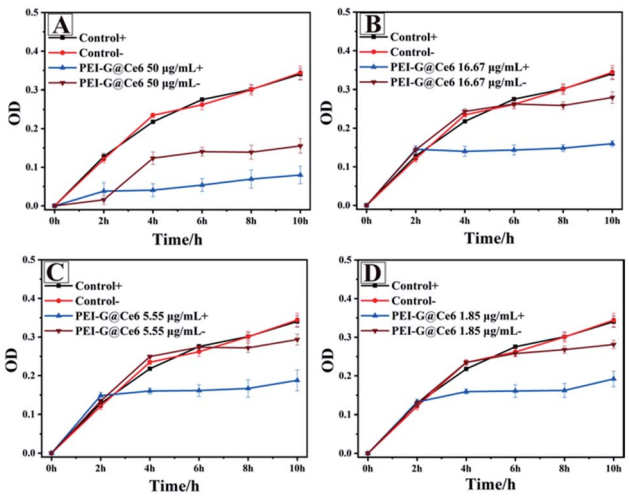

Fig. 4 *S. aureus* inhibition by PEI-G@Ce6 with a concentration of 50.00 (A), 16.67 (B), 5.55 (C) and 1.85 (D) μg mL^{-1} (+ is the illumination group, − is the non-illumination group and the control group has no PEI-G@Ce6 added).

in Fig. 4. It could be clearly seen that the illumination group displayed strong inhibitory effect towards *S. aureus* than non-illumination group at all concentrations. Under the illumination, the attached photosensitizer Ce6 on PEI-G@Ce6 can produce numerous reactive oxygen species (ROS) such as $^1O_2$ that can kill the *S. aureus* bacteria through a photodynamic process. However, it was interesting that the physical antibacterial effect of PEI-G was also observed at a high concentration of 50 μg mL^{-1} (2 h in Fig. 4A). Moreover, for the illumination group (PEI-G@Ce6 50 μg mL^{-1} +), there was an overlap of the physical antibacterial effect of PEI-G and the photodynamic antibacterial effect of Ce6. Under the dual enhancement of this double antibacterial effect, high concentration PEI-G@Ce6 can intensely inhibit *S. aureus* bacteria.

In order to further assess the survival rate of bacteria, the plate count experiment was performed after the O.D. measurement for the detection of live bacteria. Similarly, high inhibition effect on the *S. aureus* bacteria was also observed particularly at high concentrations of PEI-G@Ce6 (Fig. 5), which also was another obvious evident for the dual enhancement of this double antibacterial effect originating from the physical and photodynamic antibacterial effects of PEI-G@Ce6.

3.5 Wound healing effect

To explore the potential clinical application of PEI-G@Ce6, the *in vivo* antibacterial effects of PEI-G@Ce6 towards wound healing of mice was evaluated using Balb/c mice as a model. A wound was first introduced to the back of each mice, followed by infecting with *S. aureus*. Then, all mice were randomly divided into four groups in which three groups were treated with PEI-G@Ce6 (50 μg mL^{-1}), PEI-G (50 μg mL^{-1}) and Ce6 (17 μg mL^{-1}), respectively, followed by a 30 min illumination with 650 nm laser light, and the last group was used as the control group without any treatment. During the course of the treatment, it can be seen that the wounds were easily formed scars and showed a better recovery pattern for the PEI-G@Ce6 group than other groups (Fig. 6A). Moreover, as listed in Table S2† of the wound size and percentage of wound healing at different days, the PEI-G@Ce6 group showed fine antibacterial effect, the wound size decreased to 10.35 mm from 100.00 mm and the percentage of wound healing reached 89.65% on the 13th day, which was better than that of amoxicillin reported in literature.[22] In addition, according to the experiment, the minimal inhibitory concentration (MIC) and minimum killing concentration (MKC) of PEI-G@Ce6 were also estimated to be 4 μg

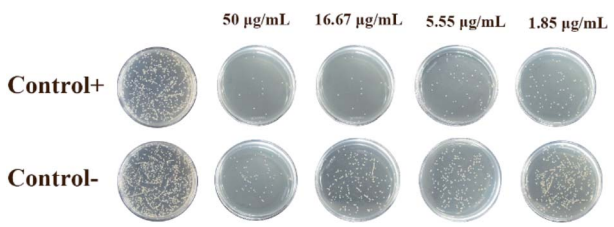

Fig. 5 Photoscopic images of *S. aureus* after being treated with PEI-G@Ce6 (50, 16.67, 5.55 and 1.85 μg mL^{-1}) with (+) and without (–) illumination.

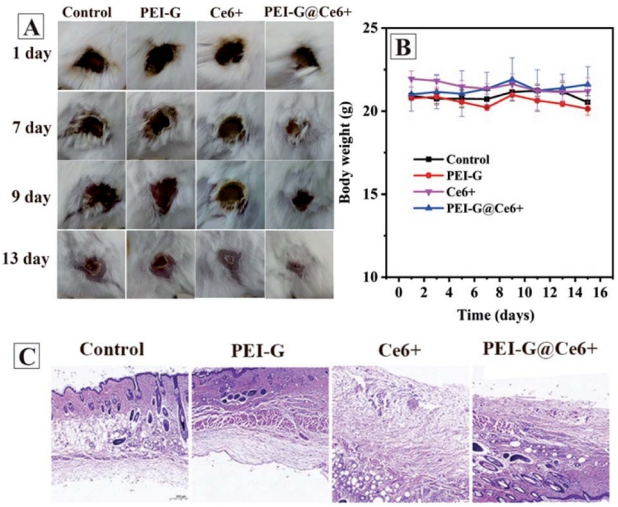

Fig. 6 *In vivo S. aureus* infected wound healing evaluation. (A) Digital images of wounds, (B) body weight change and (C) haematoxylin and eosin stain images of the wound for mice in all experimental groups.

mL^{-1} and 21 μg mL^{-1}, respectively, which were worse than that of amoxicillin reported in literature (MIC was 0.42 μg mL^{-1} and MKC was 0.56 μg mL^{-1}).[23] Moreover, the weight of mice in all groups were kept in the normal range (Fig. 6B). The H&E staining analysis was a principal stain in histology to show the general layout and distribution of cells and provide a general overview of a tissue sample's structure. Fig. 6C shows the H&E staining image of the wound issue harvested from mice treated with PEI-G, Ce6 (with illumination) and PEI-G@Ce6 (with illumination). It can be seen that compared to the control group all groups showed clear cell nuclei (blue), extracellular matrix and cytoplasm (pink), which revealed a complete and intact skin structure. Furthermore, there was also no noticeable damage or inflammatory lesion in major organs of mice in the PEI-G@Ce6 group (Fig. S4†). Therefore, the PEI-G@Ce6 was non-toxic apart from having little side-effects and it displayed sufficient therapeutic effects for the infection of *S. aureus* than Ce6 under the dual enhancement of the physical and photodynamic antibacterial effects of PEI-G@Ce6.

4. Conclusions

In conclusion, this research developed a novel nano-material based antimicrobial strategy by loading a photosensitizer Ce6 onto PEI-functionalized graphene against *S. aureus*. The as-prepared PEI-G@Ce6 not only improved the photostability of free photosensitizer Ce6 molecules, but also maintained the ability of the singlet oxygen generation. Based on the dual enhancement of the physical antibacterial effects of the PEI-G and photodynamic antibacterial effects of Ce6, the PEI-G@Ce6 nano-composite displayed adequate *in vitro* and *in vivo* antimicrobial activity against *S. aureus* and obtained satisfactory wound healing therapeutic effects than Ce6. Therefore, this dual enhancement strategy paved a new way to broaden the potential applications of nano-material based photodynamic therapeutics in clinical research.

Conflicts of interest

There are no conflicts to declare.

Acknowledgements

The authors acknowledge the support provided by the National Natural Science Foundation of China (No. 31870078 and 21802009), Second Tibetan Plateau Scientific Expedition and Research Program (STEP) (No. 2019QZKK0201), Collaboration and Innovation on New Antibiotic Development and Industrialization of Chengdu Science and Technology Bureau (NO. 2016-XT00-00023-GX) and the Natural Science Foundation of Zhejiang Provincial (No. LY18B050005). The author also thanks the friendly help of China Novel Antibiotics Cultural Collection Center.

Notes and references

1 S. U. Vetterli, K. Moehle and J. A. Robinson, *Bioorg. Med. Chem.*, 2016, **24**, 6332–6339.
2 L. Zimmermann, I. Das, J. Désiré, G. Sautrey, V. Barros R. S., M. El Khoury, M.-P. Mingeot-Leclercq and J.-L. Décout, *J. Med. Chem.*, 2016, **59**, 9350–9369.
3 T. Chalopin, D. Alvarez Dorta, A. Sivignon, M. Caudan, T. I. Dumych, R. O. Bilyy, D. Deniaud, N. Barnich, J. Bouckaert and S. G. Gouin, *Org. Biomol. Chem.*, 2016, **14**, 3913–3925.
4 Y. Yang, H. Hu, L. Chen, H. Bai, S. Wang, J.-F. Xu and X. Zhang, *Mater. Chem. Front.*, 2019, **3**, 806–811.
5 C. Lan and S. Zhao, *J. Mater. Chem. B*, 2018, **6**, 6685–6704.
6 T. Liu, C. Wang, W. Cui, H. Gong, C. Liang, X. Shi, Z. Li, B. Sun and Z. Liu, *Nanoscale*, 2014, **6**, 11219–11225.
7 M. Hoseinnejad, S. M. Jafari and I. Katouzian, *Crit. Rev. Microbiol.*, 2018, **44**, 161–181.
8 A. Raghunath and E. Perumal, *Int. J. Antimicrob. Agents*, 2017, **49**, 137–152.
9 J. Cheng, G. Tan, W. Li, H. Zhang, X. Wu, Z. Wang and Y. Jin, *New J. Chem.*, 2016, **40**, 8522–8534.
10 Z. Zhao, R. Yan, J. Wang, H. Wu, Y. Wang, A. Chen, S. Shao and Y.-Q. Li, *J. Mater. Chem. B*, 2017, **5**, 3572–3579.
11 H. Y. Mao, S. Laurent, W. Chen, O. Akhavan, M. Imani, A. A. Ashkarran and M. Mahmoudi, *Chem. Rev.*, 2013, **113**, 3407–3424.
12 S. Panda, T. K. Rout, A. D. Prusty, P. M. Ajayan and S. Nayak, *Adv. Mater.*, 2018, **30**, 1702149.
13 M. Engel, D. B. Farmer, J. T. Azpiroz, J.-W. T. Seo, J. Kang, P. Avouris, M. C. Hersam, R. Krupke and M. Steiner, *Nat. Commun.*, 2018, **9**, 4095.
14 T.-W. Lin, T.-T. Tasi, P.-L. Chang and H.-Y. Cheng, *ACS Appl. Mater. Interfaces*, 2016, **8**, 8315–8322.
15 X. Pang, Q. Xiao, Y. Cheng, E. Ren, L. Lian, Y. Zhang, H. Gao, X. Wang, W. Leung, X. Chen, G. Liu and C. Xu, *ACS Nano*, 2019, **13**, 2427–2438.
16 R. Mortensen, H. S. Clemmensen, J. S. Woodworth, M. L. Therkelsen, T. Mustafa, K. Tonby, S. Jenum, E. M. Agger, A. M. Dyrhol-Riise and P. Andersen, *Commun. Biol.*, 2019, **2**, 288.
17 C. Li, X. Wang, F. Chen, C. Zhang, X. Zhi, K. Wang and D. Cui, *Biomaterials*, 2013, **34**, 3882–3890.
18 J. He, X. Zhu, Z. Qi, C. Wang, X. Mao, C. Zhu, Z. He, M. Li and Z. Tang, *ACS Appl. Mater. Interfaces*, 2015, **7**, 5605–5611.
19 K. He, Z. Zeng, A. Chen, G. Zeng, R. Xiao, P. Xu, Z. Huang, J. Shi, L. Hu and G. Chen, *Small*, 2018, **14**, 1800871.
20 Y. Duan, Y. Yang, J. Wang, H. Li and K. Liu, *Anal. Methods*, 2020, **12**, 132–140.
21 J. H. Li, G. Wang, H. Q. Zhu, M. Zhang, X. H. Zheng, Z. F. Di, X. Y. Liu and X. Wang, *Sci. Rep.*, 2014, **4**, 4359.
22 F. I. A. El-Ela, A. A. Farghali, R. K. Mahmoud, N. A. Mohamed and S. A. A. Moaty, *Sci. Rep.*, 2019, **9**, 6418.
23 I. P. Olwoch, O. B. W. Greeff, G. Jooné and V. Steenkamp, *BMC Microbiol.*, 2014, **14**, 251.